Calculation of longitudinal polarizability and second hyperpolarizability of polyacetylene with the coupled perturbed Hartree-Fock/Kohn-Sham scheme: Where it is shown how finite oligomer chains tend to the infinite periodic polymer

Valentina Lacivita, Michel Rèrat, Roberto Orlando, Mauro Ferrero, and Roberto Dovesi

Articles you may be interested in

The calculation of the static first and second susceptibilities of crystalline urea: A comparison of Hartree–Fock and density functional theory results obtained with the periodic coupled perturbed Hartree–Fock/Kohn–Sham scheme
J. Chem. Phys. **131**, 214704 (2009); 10.1063/1.3267861

Crystal orbital calculation of coupled-perturbed Hartree–Fock dynamic (hyper)polarizabilities for polydiacetylene and polybutatriene
J. Chem. Phys. **117**, 385 (2002); 10.1063/1.1480876

Extension of the Genkin and Mednis treatment for dynamic polarizabilities and hyperpolarizabilities of infinite periodic systems. I. Coupled perturbed Hartree–Fock theory
J. Chem. Phys. **113**, 1294 (2000); 10.1063/1.481907

Assessment of conventional density functional schemes for computing the polarizabilities and hyperpolarizabilities of conjugated oligomers: An ab initio investigation of polyacetylene chains
J. Chem. Phys. **109**, 10489 (1998); 10.1063/1.477731

Correlation potentials and functionals in Hartree-Fock-Kohn-Sham theory
J. Chem. Phys. **107**, 1536 (1997); 10.1063/1.474506

Calculation of longitudinal polarizability and second hyperpolarizability of polyacetylene with the coupled perturbed Hartree-Fock/Kohn-Sham scheme: Where it is shown how finite oligomer chains tend to the infinite periodic polymer

Valentina Lacivita,[1,a)] Michel Rèrat,[2] Roberto Orlando,[1] Mauro Ferrero,[2] and Roberto Dovesi[1]

[1]*Dipartimento di Chimica, Università di Torino and NIS - Nanostructured Interfaces and Surfaces, Centre of Excellence, Via P. Giuria 7, 10125 Torino, Italy*
[2]*Equipe de Chimie Physique, IPREM UMR5254, Universitè de Pau, 64000 Pau, France*

The longitudinal polarizability, α_{xx}, and second hyperpolarizability, γ_{xxxx}, of polyacetylene are evaluated by using the coupled perturbed Hartree-Fock/Kohn-Sham (HF/KS) scheme as implemented in the periodic CRYSTAL code and a split valence type basis set. Four different density functionals, namely local density approximation (LDA) (pure local), Perdew-Becke-Ernzerhof (PBE) (gradient corrected), PBE0, and B3LYP (hybrid), and the Hartree-Fock Hamiltonian are compared. It is shown that very tight computational conditions must be used to obtain well converged results, especially for γ_{xxxx}, that is, very sensitive to the number of $\vec{k}$ points in reciprocal space when the band gap is small (as for LDA and PBE), and to the extension of summations of the exact exchange series (HF and hybrids). The band gap in LDA is only 0.01 eV: at least 300 $\vec{k}$ points are required to obtain well converged total energy and equilibrium geometry, and 1200 for well converged optical properties. Also, the exchange series convergence is related to the band gap. The PBE0 band gap is as small as 1.4 eV and the exchange summation must extend to about 130 Å from the origin cell. Total energy, band gap, equilibrium geometry, polarizability, and second hyperpolarizability of oligomers $-(C_2H_2)_m-$, with m up to 50 (202 atoms), and of the polymer have been compared. It turns out that oligomers of that length provide an extremely poor representation of the infinite chain polarizability and hyperpolarizability when the gap is smaller than 0.2 eV (that is, for LDA and PBE). Huge differences are observed on α_{xx} and γ_{xxxx} of the polymer when different functionals are used, that is in connection to the well-known *density functional theory (DFT) overshoot*, reported in the literature about short oligomers: for the infinite model the ratio between LDA (or PBE) and HF becomes even more dramatic (about 500 for α_{xx} and 10^{10} for γ_{xxxx}). On the basis of previous systematic comparisons of results obtained with various approaches including DFT, HF, Moller-Plesset (MP2) and coupled cluster for finite chains, we can argue that, for the infinite chain, the present HF results are the most reliable. © *2012 American Institute of Physics*. [http://dx.doi.org/10.1063/1.3690457]

I. INTRODUCTION

It is well-known that, in Kohn-Sham density functional theory (KS-DFT), conventional functionals lead to a large overshoot for the calculated longitudinal static electronic polarizability and hyperpolarizabilities of extended quasi-linear chains. The classic example is that of π-conjugated polyene oligomers,[1,2] but this result has been confirmed for many other cases with and without π-conjugation.[3–7] The oligomer chain lengths that have been considered typically show slight convergence of the (hyper)polarizability per unit of C_2H_2, or even no convergence, of the KS-DFT calculations towards the infinite polymer limit. Thus, the macroscopic long chain behavior and the limiting values of the (hyper)polarizabilities are unknown.

On the other hand, in principle it should be feasible to carry out infinite periodic polymer calculations directly us-

ing one of the many periodic codes now publicly available. A complementary condition is however the availability of computational tools for the calculation of the polarizability and hyperpolarizability in a *coupled* form that permits electrons to relax under the effect of the perturbation.

These conditions are fulfilled by a development version of the periodic quantum mechanical CRYSTAL code,[8] in which the coupled perturbed Hartree-Fock and Kohn-Sham (CPHF and CPKS) schemes are implemented up to second order perturbation in the wave-function (see for example Ref. 9), as alternative to the variational finite-field method providing the field-dependent energy.

In this paper we utilize the CRYSTAL code to perform electronic (hyper)polarizability calculations on long chain polyenes and on infinite periodic polyacetylene (PA) at the Hartree-Fock (HF) and KS-DFT levels. For KS-DFT, several representative conventional hybrid and non-hybrid functionals are employed. The infinite periodic KS-DFT calculations, in particular, represent a severe test of the methodology as

a)Electronic mail: valentina.lacivita@unito.it.

well as the accuracy that can be achieved. In this connection it is important to note that there are major differences in both the physics and the formal theory when one switches from a finite to an infinite periodic chain.[10,11] Hence, the consistency of the results obtained for these two cases is not guaranteed, and the computational conditions that ensure convergence must be verified carefully. Our aim is to build a robust computational scheme for the calculation of optical properties, even in cases at the limit of conductivity. In doing so, we show that it is possible to draw regular $0D \rightarrow 1D$ trends (without border effects for finite chains) at every level of theory, regardless the convergence rates and the magnitude of the numbers to manage. In addition, cases where the polymer asymptote is approached, the finite chain results extrapolate perfectly to the infinite periodic chain limit. The basis set effect is also explored.

The paper is organized as follows: in Sec. II, the basic periodic CPHF/KS equations are shortly recalled. In Sec. III, the computational details are illustrated. In particular, the most delicate computational parameters of periodic calculations, namely the number of $\vec{k}$ points at which the self-consistent field (SCF) and CPHF equations are solved and the parameters controlling the truncation of the exact exchange series are discussed. The results are presented in Sec. IV: (a) convergence of the oligomers to the polymer for various properties, including α and γ; (b) the comparison of the five different levels of theory here explored; and (c) the effect of the basis set. Finally, in Sec. V, a few conclusions are drawn.

II. THE CPHF/CPKS METHOD TO FOURTH ORDER

(Hyper)polarizability tensors can be calculated as derivatives of the total energy E_{tot} with respect to the electric field components ε_t ($t = 1, 2, 3$). Analytical formulas for estimating these derivatives are provided by the CPHF/KS method,[12] as adapted for periodic systems,[13] and recently implemented[9,14–16] for $0D$ to $3D$ systems in a local variational basis within the CRYSTAL code.[8]

Basically, the scheme focuses on the description of the crystalline orbitals (CO) relaxation under the effect of the field,

$$\frac{\partial^n C_j}{\partial \varepsilon_{t_1} \dots \partial \varepsilon_{t_n}} \equiv C_j^{(t_i \dots t_n)} = \sum_j U_{ij}^{(t_i \dots t_n)} C_i^{[0]}, \quad (1)$$

- $U^{(t_i \dots t_n)}$ being the unknown matrix which transforms the unperturbed coefficients $C^{[0]}$ (see Ref. 12) - and uses the perturbed wave functions to calculate the dielectric properties as energy derivatives.

Previous works[9,15] on periodic systems led us to the following coupled perturbative expressions for:

1. The static polarizability α

$$\alpha_{tu} \equiv -\frac{\partial^2 E_{tot}}{\partial \varepsilon_t \partial \varepsilon_u} = -\frac{2}{n_k} \Re \left(P_{t,u} \sum_{\vec{k}}^{BZ} \sum_a \sum_p \Xi_{ap}^{(t)} U_{pa}^{(u)} \right), \quad (2)$$

2. and the static second hyperpolarizability γ

$$\gamma_{tuvw} \equiv -\frac{\partial^4 E_{tot}}{\partial \varepsilon_t \partial \varepsilon_u \partial \varepsilon_v \partial \varepsilon_w} = -\frac{1}{n_k} \Re \sum_{\vec{k}}^{BZ} \sum_a P_{t,u,v,w}$$

$$\times \left[\sum_p U_{pa}^{(t)*} \left(\sum_i G_{pi}^{(u)} U_{ia}^{(vw)} - \sum_q U_{pq}^{(vw)} G_{qa}^{(u)} \right. \right.$$

$$\left. + \frac{1}{2} \sum_q W_{pq}^{(uv)} U_{qa}^{(w)} - \frac{1}{2} \sum_b U_{pb}^{(w)} E_{ba}^{(uv)} \right)$$

$$\left. + \iota \sum_p U_{pa}^{(vw)*} \frac{\partial U_{pa}^{(t)}}{\partial k_u} \right]. \quad (3)$$

All matrices are in the unperturbed CO basis; indices i, j, l refer to generic COs whereas Roman subscripts a, b, c and p, q, r distinguish occupied and virtual COs, respectively. Dependence upon $\vec{k}$ points has been omitted for brevity. Each matrix must be understood as $\vec{k}$-dependent, e.g., $U \equiv U(\vec{k})$. In the above equations:

- n_k is the number of k points in the first Brillouin zone at which the CPHF/KS equations are solved.
- $\Re$ is the real part of the expression that follows in parentheses.
- $P_{t,u}$ is the sum of all permutations of the Cartesian field components, t and u, separated by commas (and so is $P_{t,u,v,w}$).
- $\Xi_{ij}^{(t)}$ is the tth component of the perturbation operator,

$$\hat{\Omega}(\vec{k}) = e^{\iota \vec{k} \cdot \vec{r}} \vec{\nabla}_{\vec{k}} \, e^{-\iota \vec{k} \cdot \vec{r}}, \quad (4)$$

(see Refs. 13 and 17–21) in the unperturbed CO basis; it is computed initially in the Bloch atomic orbital basis and then transformed to the CO basis using:

$$\Xi_{ij}^{(t)} = \sum_{\mu,\nu} C_{\mu i}^{[0]*} \Omega_{\mu\nu}^{(t)} C_{\nu j}^{[0]}, \quad (5)$$

- $W_{ij}^{(t)}$ and $W_{ij}^{(tu)}$ are, in order, the first and second derivatives of the two-electron interaction matrix, obtained by multiplying the bielectronic integrals with the first- and second-order perturbed density matrices:

$$D_{\mu\nu}^{(t)} = \sum_a \left(C_{\mu a}^{(t)*} C_{\nu a}^{[0]} + C_{\mu a}^{[0]*} C_{\nu a}^{(t)} \right), \quad (6)$$

$$D_{\mu\nu}^{(tu)} = \sum_a \left(C_{\mu a}^{(tu)*} C_{\nu a}^{[0]} + P_{t,u} C_{\mu a}^{(t)*} C_{\nu a}^{(u)} + C_{\mu a}^{[0]*} C_{\nu a}^{(tu)} \right). \quad (7)$$

- $G_{ij}^{(u)}$ is the derivative of the Fock matrix with respect to the u component of the applied electric field. It is a sum of two terms,

$$G_{ij}^{(u)} = \Xi_{ij}^{(u)} + W_{ij}^{(u)}. \quad (8)$$

It depends on $U^{(u)}$ through the first-order density matrix $D_{\mu\nu}^{(u)}$.

- Matrix $E^{(uv)}$ collects the second derivatives of the eigenvalues. It is obtained through a *non-canonical* process of block diagonalization by $U^{(u)}$ and $U^{(uv)}$, which leads to definition,

$$E_{ab}^{(uv)} = U_{ab}^{(uv)}(E_a - E_b) + P_{u,v}\sum_p G_{ap}^{(u)}U_{pb}^{(v)} + W_{ab}^{(uv)}, \tag{9}$$

for the occupied-occupied elements, for example.

- $\frac{\partial U_{pa}^{(t)}}{\partial k_u}$ is evaluated analytically.[13]

CRYSTAL provides self-consistent solutions to Eqs. (2) (CP-SC1) and (3) (CP-SC2), by exploiting equalities,

$$U_{ab}^{(u)} = 0, \tag{10}$$

$$U_{ab}^{(tu)} = -\frac{1}{2}P_{t,u}\sum_p U_{pa}^{(t)*}U_{pb}^{(u)}, \tag{11}$$

for block-diagonal terms, and

$$U_{ap}^{(u)} = \frac{G_{ap}^{(u)}}{E_p - E_a}, \tag{12}$$

$$U_{ap}^{(tu)} = \frac{W_{ap}^{(tu)} + P_{t,u}\left(\sum_b G_{ab}^{(t)}U_{bp}^{(u)} - \sum_q U_{aq}^{(u)}G_{qp}^{(t)} + \imath\frac{\partial U_{ap}^{(u)}}{\partial k_t}\right)}{E_p - E_a}, \tag{13}$$

for the others which involve the difference between the unperturbed eigenvalues E_a and E_p, and the derivatives $W_{ij}^{(t)}$ and $W_{ij}^{(tu)}$, which depend, respectively, on $U_{ij}^{(t)}$ and $U_{ij}^{(tu)}$ through the perturbed density matrices.[9,16]

The KS-DFT calculation of energy derivatives through Eqs. (2) and (3) using a hybrid functional, such as PBE0, have been discussed at length in Ref. 22. Interested readers are referred to that paper for details. Local density approximation (LDA) and Perdew-Becke-Ernzerhof (PBE) can be seen as particular cases of the general derivation.

III. COMPUTATIONAL DETAILS

Calculations have been performed using a development version of the periodic *ab initio* CRYSTAL09 code,[8] that adopts a Gaussian-type basis set for constructing the Bloch functions, that are the variational basis for building the COs. Most of the calculations have been performed by using a 6-31G (all-electron) split-valence basis set, relying on the good accuracy of static longitudinal results previously obtained for long chain polyenes:[12,23] the longer the chain, the higher the compensation of neighboring atomic functions for the lack of extended polarization functions.[12] It consists of nine atomic orbitals (AO) resulting from a contraction of 6(s), 3(sp), and 1(sp) Gaussian-type functions for C and 2s type AO (3G and 1G contractions) for H. Much larger basis sets have then been used in order to verify the effect on all the considered properties.

Five different levels of theory have been compared, namely (i) pure density functional within the LDA (Refs. 24–26) or (ii) generalized gradient approximation (GGA) in the PBE (Refs. 27–30) formulation; (iii) PBE0 and (iv) B3LYP hybrid functionals with 25%(Ref. 31) and 20% (Refs. 32–34) of exact exchange, respectively, and finally (v) pure HF.

Convergence thresholds on the SCF energy and CP-SC properties have been set to $T_E = 11$ and $T_{CP} = 4$, respectively. Two kinds of parameters are critical for the calculation of the polarizability and hyperpolarizability tensors: the shrinking factor S, defining the number of $\vec{k}$ points at which the SCF and CPKS equations are solved, and the set of tolerances controlling the accuracy of the Coulomb and Hartree-Fock exchange series (the latter being relevant for HF, B3LYP, and PBE0).

A. Convergence with respect to the number of $\vec{k}$ points

We first check the influence of the shrinking factor S on the SCF equilibrium solution (total energy E_{tot}, interatomic distances L, band gap E_g, Mulliken bond population BP), as shown in Table I. PBE and B3LYP data are not reported, as the former exhibits a trend similar to LDA and the latter to PBE0. It turns out that for the HF solution, which is characterized by a band gap E_g as large as 6.80 eV, $S = 30$ - corresponding to 16 $\vec{k}$ points in the irreducible Brillouin zone, due to time reversal symmetry - already provides well converged values for all the considered quantities. At the other extreme, the LDA band gap is very small (of the order of 0.08 eV); as a consequence, the convergence with S is extremely slow and only at $S = 300$

TABLE I. Total energy and equilibrium geometry of PA as functions of the shrinking factor S. E_g is the energy gap (in eV) and ΔE (in microhartree) the energy difference with respect to the most accurate results, i.e., -76.86124747 hartree (HF), -77.29556515 hartree (PBE0), and -76.67436338 hartree (LDA). Interatomic distances (L) in Å and Mulliken bond populations (BP) in $|e|$. A 6-31G type basis set has been used. Other computational parameters (see text for details): $T_E = 11$, $T_C = 10$, and $T_x = 30$.

	S	E_g	ΔE	$C_1 = C_2$		$C_2 - C_3$	
				L	BP	L	BP
HF	30	6.792	0.00	1.338	0.591	1.452	0.376
	40	6.792	…	1.338	0.591	1.452	0.376
	30	1.426	5.19	1.368	0.512	1.426	0.407
	40	1.415	0.66	1.368	0.512	1.426	0.407
PBE0	50	1.412	0.09	1.368	0.512	1.426	0.407
	60	1.412	0.01	1.368	0.512	1.426	0.407
	80	1.412	0.00	1.368	0.512	1.426	0.407
	100	1.412	…	1.368	0.512	1.426	0.407
	30	0.215	141.86	1.381	0.451	1.406	0.407
	40	0.180	67.14	1.383	0.447	1.403	0.411
	50	0.155	39.28	1.384	0.445	1.402	0.413
	60	0.139	24.99	1.385	0.443	1.401	0.414
	80	0.120	11.75	1.386	0.441	1.400	0.417
LDA	100	0.106	6.36	1.387	0.440	1.399	0.418
	200	0.076	0.67	1.388	0.437	1.398	0.420
	300	0.076	0.09	1.388	0.437	1.397	0.421
	400	0.076	0.02	1.388	0.436	1.397	0.421
	500	0.076	0.00	1.388	0.436	1.397	0.421
	700	0.076	…	1.388	0.436	1.397	0.421

TABLE II. Polarizability α_{xx} and second hyperpolarizability γ_{xxxx} (in a.u.) of PA as functions of the shrinking factor S. γ_{xxxx} in 10^6 (HF), 10^9 (PBE0), and 10^{16} (LDA) a.u. $T_{CP} = 4$. Basis set and other computational parameters as in Table I. Bold lines define α_{xx} and γ_{xxxx} values converged to at least 1%.

	S	$\alpha_{xx}(\times 10^2)$	γ_{xxxx}
HF	**30**	**1.629**	**5.648**
	40	1.629	5.661
PBE0	50	7.595	1.531
	60	7.545	1.837
	70	7.532	1.970
	80	7.529	2.022
	100	**7.528**	**2.046**
	150	7.528	2.049
LDA	300	1488	-0.443
	400	1250	-0.079
	500	1155	0.355
	600	1120	0.739
	700	1107	1.008
	800	1102	1.169
	900	1101	1.254
	1000	1100	1.296
	1100	1100	1.315
	1200	**1100**	**1.323**
	1250	1100	1.326

the total energy is converged to better than 10^{-7} hartree. As expected PBE0, with an intermediate E_g (1.36 eV), which is very close to the experimental value[35] ($1.6 \leq E_g \leq 1.8$ eV), converges with $S = 50$ to $\Delta E \leq 10^{-7}$ hartree.

Dependence on the shrinking factor S is also important for the polarizability α_{xx} and the second hyperpolarizability γ_{xxxx}. Two coupled perturbed (CP-SC1 and CP-SC2) iterative schemes have been carried out to achieve the fourth order of perturbation through the $(2n + 1)$ rule. Given the inverse relationship between optical constants and powers of the energy gap E_g - Eqs. (2) and (3), referring to definitions (11)–(13) - a much stronger dependence on E_g, and then on S, is to be expected, and this is actually the case, as shown in Table II, where the longitudinal components are reported. Consider first the LDA case (see also Figure 1). The variation with S is very large; α reduces by about 25% in going from $S = 300$ to $S = 700$. γ at $S = 400$ still carries the wrong sign and at $S = 600$ it is still off by 44% with respect to the converged result obtained at $S = 1200$. It should be noticed that α is as large as 10^5 and γ as large as 10^{16} in a.u. The HF solution shows a much faster convergence ($S = 30$) due to the large band-gap. Indeed, HF α is about 700 times smaller than LDA α. For γ this ratio increases to 10^{10}. About the same number of $\vec{k}$ points as used in the field-free SCF cycle, i.e., 51, is required for well converged optical properties with PBE0.

B. Convergence with respect to the two-electron series range

The effect of the five parameters controlling the truncation of the Coulomb and exchange series, indicated as T_i ($i = 1 \rightarrow 5$),[8] can be described with reference to the ex-
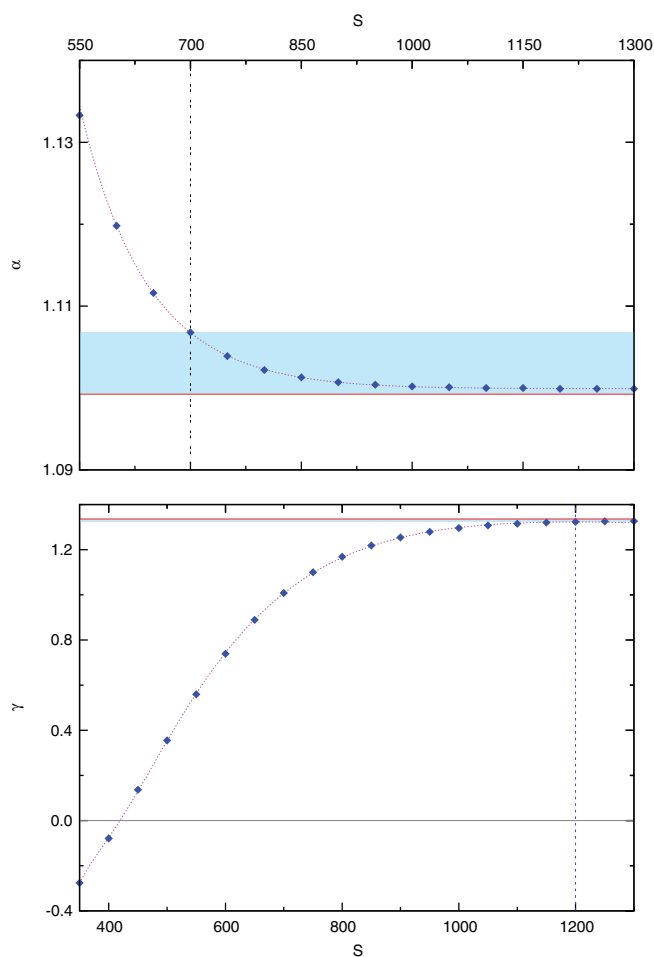

FIG. 1. LDA polarizability α_{xx} (in 10^5 a.u.) and second hyperpolarizability γ_{xxxx} (in 10^{16} a.u.) of PA as functions of the shrinking factor S. The asymptotic values are $\alpha_{xx}^{\infty} = 1.099$ and $\gamma_{xxxx}^{\infty} = 1.336$. Highlighted areas include α and γ values converged to better than 1% with respect to the asymptotes (solid lines).

pression of the total electronic energy in the AO basis:

$$E^{xc} = \frac{1}{2} \sum_{\mu\nu} \sum_{\vec{g}}^{\infty} P_{\mu\nu}^{\vec{g}} \sum_{\vec{g}'}^{\infty} \sum_{\rho\tau} P_{\rho\tau}^{\vec{g}'}$$

$$\times \sum_{\vec{g}''}^{\infty} \left[(\mu^0 \nu^{\vec{g}} | \rho^{\vec{g}''} \tau^{\vec{g}'+\vec{g}''}) - \frac{1}{2} (\mu^0 \rho^{\vec{g}''} | \nu^{\vec{g}} \tau^{\vec{g}'+\vec{g}''}) \right]. \tag{14}$$

Roughly speaking, integrals are disregarded (or approximated in the case of T_2, see below) when the *overlap* between the involved functions is below 10^{-T_i} (see Ref. 8). T_1 and T_2 refer to the Coulomb series (T_C). T_1 defines the minimum amount of charge density to be considered for electron 1 or 2. T_2 defines the set of direct space $\vec{g}$ vectors within which these bielectronic integrals are calculated exactly, otherwise a multipolar expansion is used to describe the interacting charge distributions.[36–38] The effect of T_C (here T_1 has been set equal to T_2) on the ground state and its optical properties is documented in Table III. Both α and γ show high stability with respect to T_c, so that $T_c = 10$ can be used safely (despite the small energy variation at higher T_c values), extending the

TABLE III. Polarizability α_{xx} ($\times 10^2$ a.u.) and second hyperpolarizability γ_{xxxx} (in a.u.) of PA as functions of the parameter T_C controlling the truncation of the Coulomb series (see text for details). E_g is the energy gap (in eV) and ΔE (in microhartree) the energy difference with respect to the most accurate results, i.e., -76.86126625 hartree (HF), -77.29557482 hartree (PBE0), and -76.67435270 hartree (LDA). Shrinking factor S is set to 300 (LDA), 50 (PBE0), and 30 (HF) for geometry optimizations and to 1200 (LDA), 100 (PBE0), and 30 (HF) for CPHF/KS calculations. Other computational parameters as in previous tables.

	LDA				PBE0				HF			
T_C	E_g	ΔE	α	γ ($\times 10^{16}$)	E_g	ΔE	α	γ ($\times 10^9$)	E_g	ΔE	α	γ ($\times 10^6$)
10	0.076	−10.69	1100	1.323	1.420	19.94	7.437	1.972	6.792	18.78	1.629	5.648
20	0.076	0.62	1097	1.312	1.420	0.74	7.441	1.975	6.792	1.09	1.630	5.650
30	0.076	...	1096	1.310	1.420	...	7.441	1.975	6.792	...	1.630	5.650

summation over the exact Coulomb terms to $N = 11$ (number of cells). Champagne et al.[39] observed the same rapid convergence at the HF/Slater-Type-Orbitals(STO)-3G level, referring to an equivalent space partition in short/medium- and long-range (LR) regions.

T_3, T_4, and T_5 are associated with HF exchange summations. T_3 truncates the summation over $\vec{g}''$, Eq. (14), when the overlap distributions $\{\mu^0 \rho^{\vec{g}''}\}$ or $\{\nu^{\vec{g}} \tau^{\vec{g}'+\vec{g}''}\}$ are below 10^{-T_3}. It is the equivalent of T_1, but for the exchange series. As $T_3 = 10$ provides well converged results, we use this value. More delicate is the role of T_4 and T_5, which select pseudo-overlaps $\{\mu^0 \nu^{\vec{g}}\}$ and $\{\rho^{\vec{g}''} \tau^{\vec{g}'+\vec{g}''}\}$, thus limiting summations over $\vec{g}$ and $\vec{g}'$ (see Ref. 40). They control the spatial range of the density matrix elements $P_{\mu\nu}^{\vec{g}}$ and $P_{\rho\tau}^{\vec{g}'}$ in Eq. (14), which depends in turn on the electronic structure of the system: the smaller the gap, the larger the range of the density matrix.[40] We set their values according to the scheme $T_4 = \frac{1}{2}T_5 = T_x$. SCF energy calculations converge at $T_x = 30$ and $T_x = 150$ for HF and PBE0, respectively (Table IV). Much slower is the CPHF/KS convergence, in particular for PBE0, as shown in Table V. Convergence to 1% on γ_{xxxx} is achieved at $T_x = 100$ ($N = 33$) for HF (about three times slower than what documented in Ref. 39), whereas PBE0 requires T_x as large as

1000 ($N = 103$, Figure 2), even if only a fraction of exact exchange (1/4) is incorporated in it.

The DFT exchange-correlation contribution in PBE0 and LDA is obtained by numerical integration, using a Gauss-Legendre radial quadrature and a Lebedev 2D angular scheme.[41,42] Pre-defined *pruned* grids are adopted.[8] The default grid (75 radial and 974 angular points per atom) provides well converged results for both the equilibrium geometry and the optical properties α and γ.

IV. RESULTS

A. From the molecule to the polymer: Structures, energetics, and optical properties

In this section, convergence of the acetylene oligomers $-(C_2H_2)_m-$ towards the periodic polymer (PA) will be considered. We will try to answer the following questions:

TABLE IV. Total energy and equilibrium geometry of PA as functions of the parameter T_x, controlling the truncation of the exchange series (HF and PBE0). E_g is the energy gap (in eV) and ΔE (in microhartree) the energy difference with respect to the most accurate result, i.e., -76.8612902 hartree (HF) and -77.2956558 hartree (PBE0). Symbols, units, and other computational parameters as in previous tables.

				$C_1 = C_2$		$C_2 - C_3$	
	T_x	E_g	ΔE	L	BP	L	BP
HF	30	6.792	42.72	1.3382	0.591	1.4516	0.376
	40	6.805	−0.05	1.3384	0.591	1.4512	0.376
	50	6.808	...	1.3384	0.591	1.4512	0.376
PBE0	30	1.412	90.74	1.3679	0.512	1.4259	0.407
	40	1.418	41.77	1.3682	0.511	1.4255	0.408
	50	1.420	41.22	1.3682	0.511	1.4255	0.408
	60	1.423	19.97	1.3684	0.511	1.4252	0.408
	80	1.423	9.60	1.3685	0.510	1.4250	0.408
	100	1.423	7.74	1.3685	0.510	1.4250	0.408
	120	1.426	3.00	1.3686	0.510	1.4249	0.409
	150	1.426	0.37	1.3687	0.510	1.4248	0.409
	180	1.426	0.00	1.3687	0.510	1.4248	0.409

TABLE V. Polarizability α_{xx} and second hyperpolarizability γ_{xxxx} (in a.u.) of PA as functions of the thresholds, $T_x = T_4 = \frac{1}{2}T_5$, controlling the truncation of the exchange series (see text for details). M is the number of direct lattice vectors involved in the exchange series summations, R is the *radius* (in Å) of this exchange zone. Symbols, units, and other computational parameters as in previous tables.

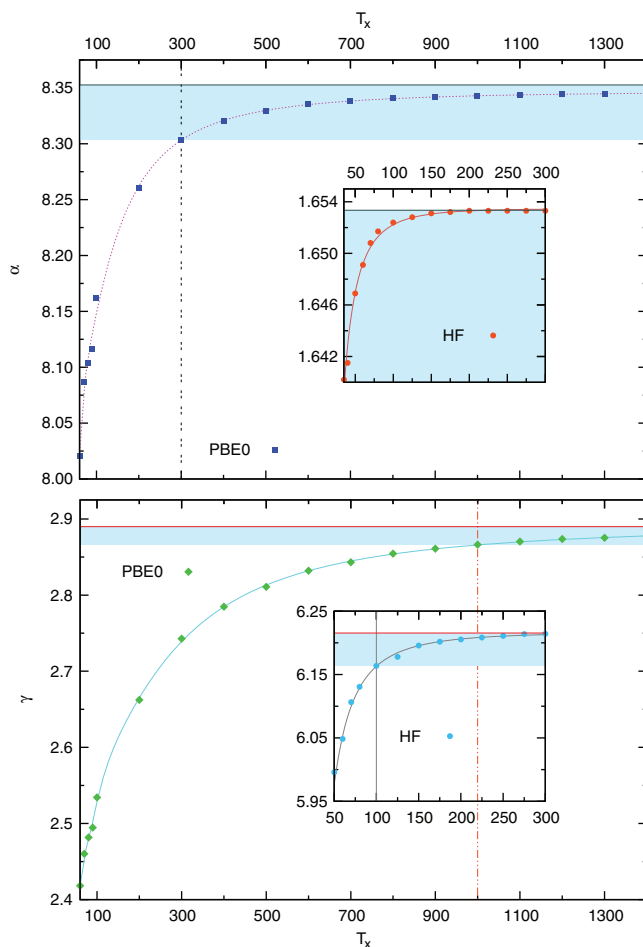|			PBE0		HF	
T_x	M	R	α	γ ($\times 10^9$)	α	γ ($\times 10^6$)
30	19	24.71	785.7	2.329	163.6	5.726
40	21	27.18	788.2	2.338	164.1	5.859
50	23	29.65	800.6	2.400	164.7	5.993
60	25	32.12	802.0	2.418	164.9	6.046
70	29	37.07	808.7	2.460	165.1	6.104
80	29	37.07	810.4	2.482	165.2	6.128
100	33	42.01	816.2	2.534	**165.2**	**6.161**
200	47	59.31	826.1	2.662	165.3	6.203
300	57	71.66	830.4	2.743	165.3	6.212
400	65	81.55	832.0	2.785	...	...
500	73	91.43	833.0	2.811	...	...
600	81	101.3	833.5	2.832	...	...
700	87	108.7	833.8	2.843	...	...
800	93	116.2	834.1	2.854	...	...
900	99	123.6	834.2	2.861	...	...
1000	103	128.5	834.3	2.866	...	...
1100	109	135.9	834.4	2.870	...	...
1200	113	140.9	834.4	2.874	...	...

FIG. 2. HF and PBE0 polarizability α_{xx} and second hyperpolarizability γ_{xxxx} of PA as functions of the thresholds T_x controlling the truncation of the exact exchange integrals series (see text for details). α_{xx} in 10^2 a.u. (PBE0 and HF); γ_{xxxx} in 10^9 (PBE0) and 10^6 (HF) a.u. The asymptotic values are $\alpha_{xx}^{\infty} = 8.353$ and $\gamma_{xxxx}^{\infty} = 2.890$ (PBE0); $\alpha_{xx}^{\infty} = 1.653$ and $\gamma_{xxxx}^{\infty} = 6.216$ (HF). Highlighted areas include α and γ values converged to better than 1% with respect to the asymptotes (solid lines).

1. How rapid is the convergence of the total energy, the equilibrium geometry, the charge distribution as a function of the number of monomers m?
2. How fast do α and γ converge? (Note that, as PA belongs to the C_{2h} point symmetry, the dipole moment μ and the first hyperpolarizability β are null due to inversion symmetry.)
3. Does convergence vary with the functionals?
4. Is the overall accuracy of the CRYSTAL code, in all its parts (SCF, CP-SC1, and CP-SC2), such as to permit us to verify the infinite oligomer chain limit by comparison with the polymer?

In previous investigations the infinite chain limit was approached with finite chains of increasing length (see, for example, Refs. 23, 43, and 44). The HF infinite limit was explored by Kirtman *et al.*[45] through periodic CPHF calculations, the results being very close to the present ones. Here, the $0D \rightarrow 1D$ analysis has been extended to DFT pure (LDA and GGA) and hybrid (PBE0 and B3LYP) functionals.

The last question is not trivial, as in Sec. III it has been shown that the influence of the computational parameters on the calculated properties is very large. The two most important possible sources of discrepancy are: (a) the strong dependence of many properties of the polymer on the shrinking factor S documented in Sec. III must take the form of a strong dependence on the chain length in $0D$ oligomers; (b) the electric field operator, that is, simply $\vec{r}$ for the $0D$ cases, along the $1D$ chain takes the form $\vec{r} + \iota \, \vec{\nabla}_k$. At the limit $m \rightarrow \infty$ the two values should coincide.

In order to eliminate border (finite chain) effects, extensive properties are evaluated as differences between oligomers of different length: for example, α (as well as E_{tot} and γ) of the *central* monomer is evaluated as $\alpha' = \alpha^m - \alpha^{m-1}$. Intensive properties - such as bond lengths and Mulliken populations in Table VI - refer to the central part of the oligomer. The band gap of the oligomer cannot be purified of border effects.

Full-geometry optimizations were carried out for m up to 50, corresponding to oligomers with as many as 202 atoms. Table VI provides energy and geometry of oligomers of increasing length (the reference polymer data are in the last row), whereas energy gaps (eV), α and γ (a.u.) values are reported in Table VII. For HF the convergence of energy and geometry is extremely rapid: at $m = 12$, the total energy (per monomer unit) is already equal to the one of the polymer up to the seventh decimal figure and the two alternating bond lengths coincide with those in the polymer to the fourth decimal digit. The polymer structure overlaps almost perfectly to the HF one obtained by Limacher *et al.*[46] using a more extended basis set, i.e., cc-pVDZ. We note a HF overshoot ($\sim$25%–30%) of the bond length alternation (BLA $= \Delta(C_1C_2 - C_2C_3) = 0.113$ Å) compared to the experimental data: BLA $= 0.085$ Å,[46] 0.08 Å,[47] and 0.086 Å.[48] On the other hand, the HF symmetry-breaking dimerization distortion value u_0 of 0.03 Å compares well with the x-ray diffraction result derived by Fincher *et al.*,[35] whereas inclusion of electron correlation fails by systematic underestimation.[49,50]

Structural properties of the oligomers converge monotonically to those for the polymer also in the LDA approximation. Convergence is, however, much slower: at $m = 50$ E_{tot} still differs by 4 microhartree and the bond lengths by about 3 mÅ. As usual, PBE0 is an intermediate case.

As expected, convergence of α_{xx} and γ_{xxxx} requires achieving larger m values than for structural and energetic properties (see Table VII). For HF, at $m = 20$, α differs from the polymer value by about 2%, and at $m = 50$ by 0.1%. These differences increase to 12% ($m = 20$) and 0.5% ($m = 50$) for γ. The good convergence is graphically documented by Figure 3. Using power series in $1/m$ as fitting functions yields $\alpha_{xx}^{\infty} = 165$ a.u. and $\gamma_{xxxx}^{\infty} = 617 \times 10^4$ a.u. for the infinite m limit, which almost coincide with the analytical (infinite periodic) CPHF results. This not only confirms the internal consistency of our method, but also lends further reliability to previous extrapolation attempted by Kirtman *et al.*[23] - who predicted α_{xx}^{∞} and γ_{xxxx}^{∞} to be, respectively, 166 ± 5 a.u. (to be compared with 165 a.u. in the present case) and $(691 \pm 39) \times 10^4$ a.u. (to be compared with 616×10^4 a.u. in the present case) - despite their extrapolation was obtained from absolute ratios α/m and γ/m without eliminating border

TABLE VI. $0D \to 1D$ convergence of $C_1 = C_2$ and $C_2 - C_3$ bond lengths (Å) and total energy E_{tot} (hartree). Oligomer structures have been cut from the polymer, saturated, and geometry optimized. Bond lengths refer to the chain center and E_{tot} is evaluated as the difference $E_{tot}^m - E_{tot}^{m-1}$ (m is the number of $-C_2H_2-$ monomers), in order to eliminate border effects.

	LDA			PBE0			HF		
m	E_{tot}	C_1C_2	C_2C_3	E_{tot}	C_1C_2	C_2C_3	E_{tot}	C_1C_2	C_2C_3
2	−76.669561	1.3455	1.4442	−77.292400	1.3423	1.4556	−76.860119	1.3275	1.4645
4	−76.672567	1.3500	1.4326	−77.294636	1.3564	1.4391	−76.861144	1.3355	1.4548
8	−76.673809	1.3733	1.4132	−77.295549	1.3643	1.4301	−76.861246	1.3379	1.4519
12	−76.674162	1.3777	1.4085	−77.295636	1.3668	1.4271	**−76.861248**	**1.3382**	**1.4516**
16	−76.674258	1.3801	1.4060	−77.295650	1.3678	1.4259	...	...	...
20	−76.674309	1.3817	1.4043	−77.295654	1.3683	1.4254	...	...	...
30	−76.674339	1.3836	1.4022	−77.295655	1.3687	1.4249	...	...	...
40	−76.674350	1.3852	1.4005	−77.295656	1.3687	1.4249	...	...	...
50	−76.674359	1.3860	1.3997	**−77.295656**	**1.3687**	**1.4248**	...	...	...
∞	−76.674363	1.3884	1.3972	−77.295655	1.3687	1.4248	−76.861248	1.3382	1.4516

effects and slightly different BLA. Comparison of our data with CPHF/6-31G values, $\alpha_{xx} = 162$ a.u. and $\gamma = 628 \times 10^4$ a.u., reported in Ref. 45 for the minimum-energy RHF/6-31G structure of the infinite polymer is even better, as well as more homogeneous.

The existence of two different series of oligomers with odd/even number of double carbon bonds converging to the same limit at $m \to \infty$ has been envisaged to explain irregularities on the trend of γ' (without border effects).[23] The present results do not support such a hypothesis, as is shown in Fig. 4 where trends α' vs m and γ' vs m are compared with those from Ref. 23 (made consistent with our definition of α' and γ'). The accurate and rigorous scheme here adopted for setting of the computational parameters (see Sec. III) has

TABLE VII. $0D \to 1D$ convergence of the polarizability α_{xx} and the second hyperpolarizability γ_{xxxx} (in a.u.) of PA. E_g (eV) is the energy gap. α in 10^3 a.u. (LDA), 10^2 a.u. (PBE0 and HF); γ in 10^{10} a.u. (LDA), 10^9 a.u. (PBE0) and 10^6 a.u. (HF). Oligomer structures have been cut from the polymer, saturated, and geometry optimized. Differences $\alpha'_{xx} = \alpha_{xx}^m - \alpha_{xx}^{m-1}$ and $\gamma'_{xxxx} = \gamma_{xxxx}^m - \gamma_{xxxx}^{m-1}$, without border effects, are reported (m is the number of $-C_2H_2-$ monomers). Basis set and computational parameters as in previous tables.

|	LDA			PBE0			HF		
m	E_g	α'_{xx}	γ'_{xxxx}	E_g	α'_{xx}	γ'_{xxxx}	E_g	α'_{xx}	γ'_{xxxx}
2	3.995	0.483	0.000	6.041	0.464	0.000	12.17	0.457	0.006
4	2.424	0.126	0.000	4.131	1.088	0.000	9.663	0.768	0.105
6	1.752	0.197	0.000	3.279	1.627	0.001	8.590	1.097	0.549
8	1.380	0.316	0.001	2.800	2.386	0.006	8.024	1.311	1.389
10	1.140	0.456	0.002	2.493	3.152	0.018	7.692	1.439	2.401
12	0.974	0.616	0.004	2.283	3.885	0.042	7.480	1.519	3.340
14	0.854	0.796	0.009	2.131	4.561	0.085	7.336	1.563	4.098
16	0.762	0.993	0.018	2.019	5.164	0.152	7.235	1.591	4.665
18	0.686	1.210	0.031	1.932	5.697	0.246	7.162	1.608	5.062
20	0.601	1.444	0.053	1.864	6.139	0.367	7.105	1.620	5.356
22	0.555	1.694	0.085	1.807	6.531	0.512	7.061	1.627	5.575
24	0.517	1.960	0.132	1.763	6.875	0.678	7.029	1.634	5.696
26	0.484	2.239	0.199	1.725	7.117	0.853	7.001	1.636	5.809
28	0.454	2.537	0.291	1.695	7.329	1.036	6.980	1.640	5.884
30	0.444	2.849	0.383	1.671	7.506	1.218	6.960	1.642	5.958
32	0.419	3.175	0.583	1.614	7.653	1.395	6.947	1.646	6.003
34	0.397	3.514	0.801	1.595	7.767	1.561	6.933	1.644	6.016
36	0.378	3.865	1.083	1.614	7.872	1.718	6.922	1.647	6.050
38	0.362	4.235	1.438	1.597	7.935	1.854	6.914	1.644	6.064
40	0.348	4.613	1.897	1.586	8.018	1.987	6.906	1.649	6.070
42	0.332	5.006	2.310	1.575	8.046	2.091	6.898	1.648	6.099
44	0.321	5.411	3.153	1.565	8.094	2.192	6.892	1.648	6.104
46	0.310	5.824	3.993	1.556	8.123	2.263	6.887	1.649	6.114
48	0.299	6.247	4.798	1.548	8.153	2.323	6.882	1.650	6.128
50	0.288	6.692	5.995	1.518	8.212	2.368	6.879	1.650	6.135
∞	0.076	110.0	1323×10^3	1.434	8.343	2.866	6.792	1.652	6.161
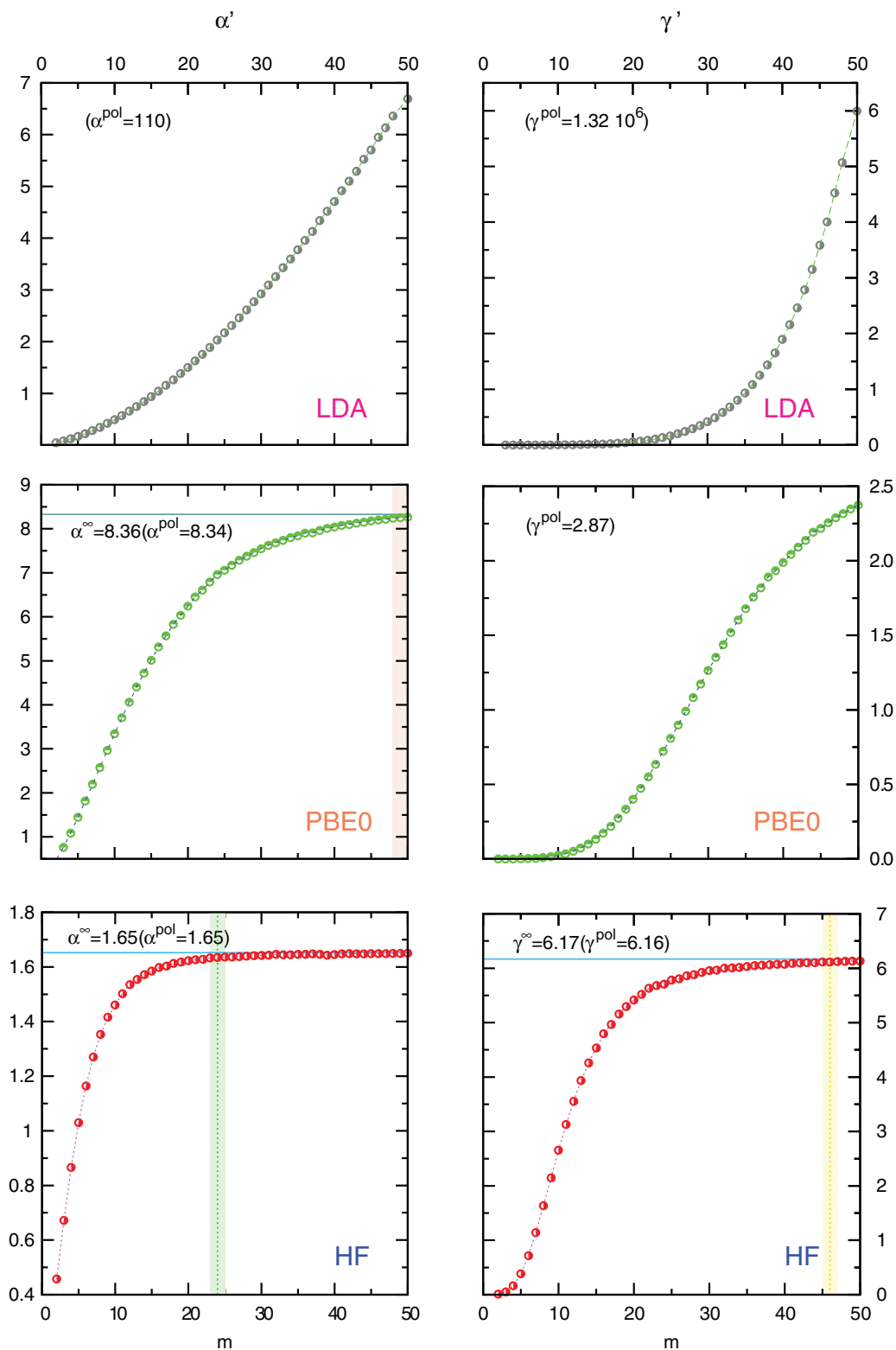
FIG. 3. $0D - 1D$ trends of the polarizability α_{xx} (left) and the second hyperpolarizability γ_{xxxx} (right) at the HF (bottom), PBE0 (center), and LDA (top) level of theory. α in 10^2 (HF and PBE0) and 10^3 (LDA) a.u.; γ in 10^6 (HF), 10^9 (PBE0), and 10^{10} (LDA) a.u. Fitting functions defined as the polynomials $\alpha' = \sum_{n=0}^{3} a_n/m^n$ and $\gamma' = \sum_{n=0}^{3} g_n/m^n$. The asymptotic values, α^∞ and γ^∞ (where existent), are compared with α^{pol} and γ^{pol} calculated for the polymer. The minimum m value providing convergence to better than 1% with respect to the asymptotes (solid lines) is highlighted.
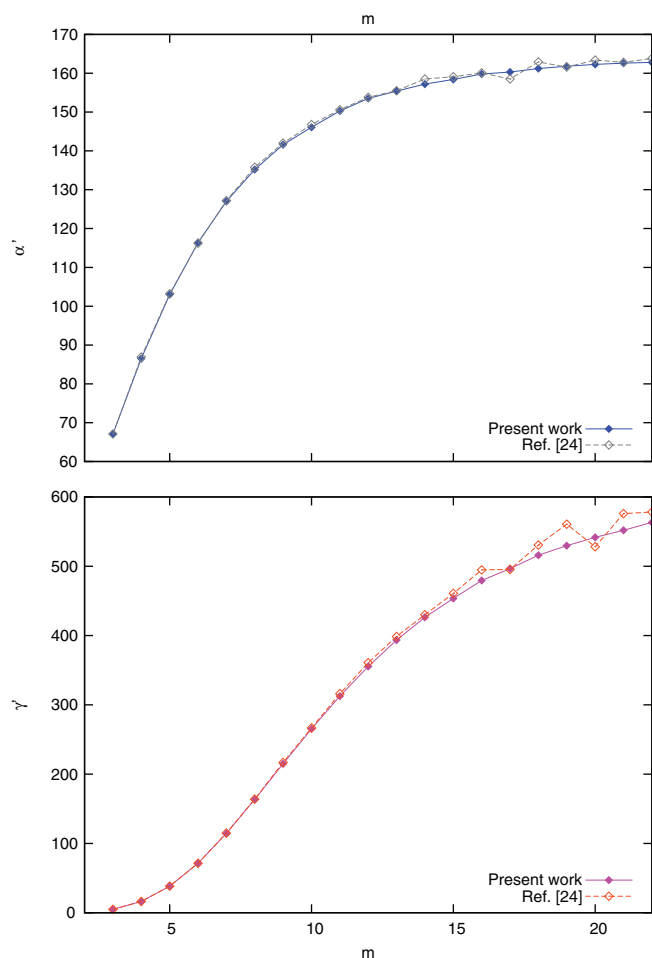
FIG. 4. Trends of the longitudinal polarizability α'_{xx} and second hyperpolarizability γ'_{xxxx} (in a.u.) of PA oligomers, $(C_2H_2)_m$, with m up to 22. Comparison between results from the present work and from Ref. 23 (obtained at the HF level) is made.

enabled us to approach the polymer limit describing a perfectly smooth pattern.

For PBE0, the E_g difference with respect to the polymer at $m = 50$ is 0.08 eV, i.e., about 6% difference from E_g in the polymer, which may be compared with the corresponding 1% difference for HF. At $m = 20$, the PBE0 α is about 25%

smaller than the converged value, and γ is only 0.4 instead of 2.87×10^9 a.u. For the largest oligomer ($m = 50$), α is within 1% of the polymer value, but γ is still off by about 20%. The difference between HF and PBE0 is evident from Figure 3, showing in particular that at $m = 50$ the gradient of the PBE0 γ curve is just starting to decrease towards the converged plateau. If the latter is estimated using the fitting function $\gamma(m) = \sum_{n=0}^{3} \frac{c_n}{m^n}$, $\gamma^{\infty}_{xxxx} = 2.49 \times 10^9$ a.u. is obtained, which still differs by about 10% from the analytical polymer value $\gamma^{pol}_{xxxx} = 2.87 \times 10^9$ a.u. However, we can still use this extrapolation procedure to predict that for $m > 60$ the calculated value will be within about 1% of the convergence limit.

Both LDA α and γ are still in the very steep part of the curve at $m = 50$, and then extremely far from convergence. Table VII documents that at $m = 50$ the α value is 6.69 $\times 10^3$ a.u., to be compared to 1.10×10^5 a.u. in the polymer, and γ is seven orders of magnitude smaller than the polymer value. The ratio $R_\alpha = \alpha^{LDA}/\alpha^{HF}$ increases from 1.22 ($m = 3$) to about 670 (polymer) - which complies with expectations on the pure DFT *catastrophe* - and the soaring ($m = 3–7$) is even higher than previous results: Karolewski *et al.*[51] report a value of R_α that increases from 1.28 ($m = 3$) to 2.00 ($m = 7$), i.e., about 10% below our estimation at $m = 7$, $R_\alpha = 2.23$. $R_\gamma = \gamma^{LDA}/\gamma^{HF}$, instead, undergoes a change of about 10 orders of magnitude: from $R_\gamma < 1$ for $m = 3 - 5$ to $R_\gamma = 2.15 \times 10^9$ at the polymer limit. At $m = 50$, we get a value of R_γ which is about 10^4, i.e., 5 orders of magnitude below the polymer limit. In this case it is impossible to extrapolate α and γ values at $m \to \infty$ from oligomers of manageable length.

B. Effect of the Hamiltonian on periodic properties

Table VIII summarizes salient data regarding the effect of the Hamiltonian. As anticipated, the LDA and PBE band gap is extremely small and, as a consequence of this quasi-metallic behavior, longitudinal α and γ components are extremely large. The convergence of oligomer properties towards the PA value is then extremely slow, due to the high electron mobility (border effects propagate into the inner chain). The iterative coupling between perturbation and CO relaxation through the CP-SC1 cycle - Eq. (12) - improves the sum over states (SOS) results for α (obtained at itera-

TABLE VIII. Bond lengths $C_1 = C_2$ and $C_2 - C_3$ (Å), cell parameter a (Å), energy gap E_g (eV) and the coupled perturbed polarizability α_{xx} and second hyperpolarizability γ_{xxxx} (in a.u.) of PA as functions of the level of theory adopted for calculations. Sum over state (SOS) values for α_{xx} and γ_{xxxx} are also shown. Basis set and computational parameters as in previous tables. PBE calculations performed using computational parameters as set for LDA; B3LYP as for PBE0.

	LDA	PBE	B3LYP	PBE0	HF
C_1C_2	1.388	1.399	1.374	1.368	1.338
C_2C_3	1.397	1.412	1.427	1.426	1.452
a	2.465	2.487	2.479	2.471	2.467
E_g	0.076	0.114	1.167	1.412	6.805
α^{SOS}_{xx}	1.280×10^5	5.874×10^4	8.438×10^2	6.146×10^2	5.659×10
α_{xx}	1.100×10^5	5.034×10^4	1.069×10^3	8.343×10^2	1.652×10^2
γ^{SOS}_{xxxx}	1.360×10^{16}	1.298×10^{15}	3.410×10^9	1.296×10^9	5.130×10^5
γ_{xxxx}	1.323×10^{16}	1.267×10^{15}	6.515×10^9	2.866×10^9	6.161×10^6

tion zero of the CP-SC1 process) by about 30% (LDA) and 15% (PBE), but still is unable to scale its magnitude. At the second order of perturbation, the effect of the CP-SC2 cycle - Eq. (13) - on γ^{SOS} is further reduced to about 2%-3% at both the LDA and PBE levels.

When the band gap is relatively large, as predicted by HF, calculated values are considerably resized in magnitude. Electron relaxation increases α^{SOS} by about a factor of 3 (so reducing the difference with respect to LDA) and γ^{SOS} by 12 times, but this is overall a minor effect as far as the DFT catastrophe is concerned. Therefore, the choice of a functional able to provide a reasonable band gap seems to be a crucial step for obtaining reliable polarizabilities and hyperpolarizabilities.

A correlation between the band gap E_g and the magnitude of α_{xx} and γ_{xxxx} (as well as the $0D \rightarrow 1D$ convergence rate) has been inferred on the basis of the data discussed above (Table VIII). However, such data correspond to a discrete sampling over a heterogeneous choice of the Hamiltonians. In order to investigate such correlation in a homogeneous framework, including the full range of possible band gaps, we performed a set of calculations in which the percentage of HF exchange X_{HF} varies continuously from 0% to 100% in the PBE functional. The computational parameters for both geometry relaxation (minimum energy structures are indicated as R_{min}) and CPKS calculations have been set according to the most stringent standards defined in Sec. III, in order to ensure sufficient stability of the results along the whole range of X_{HF} explored. Results are shown in Fig. 5 - series Fit(R_{min}). The energy gap increases from 0.114 eV when $X_{HF} = 0\%$ to 6.68 eV when $X_{HF} = 100\%$. Correspondingly, α_{xx} decreases from 50 338 to 168 a.u. and γ_{xxxx} from 1.27×10^{15} to 7.45×10^6 a.u. The values of α_{xx} and γ_{xxxx} provided by LDA, B3LYP, and HF, all reported in Fig. 5 with colored spots (PBE and PBE0 belong to the curve), lie very close to the interpolating curves $\alpha_{xx}(E_g; R_{min})$ and $\gamma_{xxxx}(E_g; R_{min})$. Figure 5 establishes a strong dependence of the (hyper)polarizabilities on the band gap, almost irrespective of the peculiarities of the various levels of theory adopted (see, for example, LDA and PBE, having both $X_{HF} = 0$ but different band gap values). Differences between α_{xx} and γ_{xxxx} values calculated with different Hamiltonians and those estimated at the same band gaps using the fitting curves $\alpha_{xx}(E_g; R_{min})$ and $\gamma_{xxxx}(E_g; R_{min})$ (Table IX) are maintained up to around 15%. Moreover, given that even the HF data are consistent with the fitting, we can extend the argument of the minority *short-range* role of correlation potential (with respect to the exchange potential) in the calculation of the optical properties of small band gap finite systems[3] to periodic systems.

In Sec. III (Tables I and IV) it is shown that the band gap (and thus also α_{xxxx} and γ_{xxxx}) is closely related to the pattern of alternating bonds in PA. Indeed, if we run all the CPKS calculations represented in Fig. 5 - series Fit(R_{min}) at the same geometry (for example, that obtained for PBE) the resulting curve, Fig. 5 - series Fit(R_{PBE}), deviates significantly from the first. Comparison between curves Fit(R_{min}) and Fit(R_{PBE}) clearly shows that the band gap and the bond lengths are strongly correlated, and we can restrict the dependence of α_{xx} and γ_{xxxx} essentially on a single parameter. Consider, for example, the case $X_{HF} = 25\%$, i.e., a
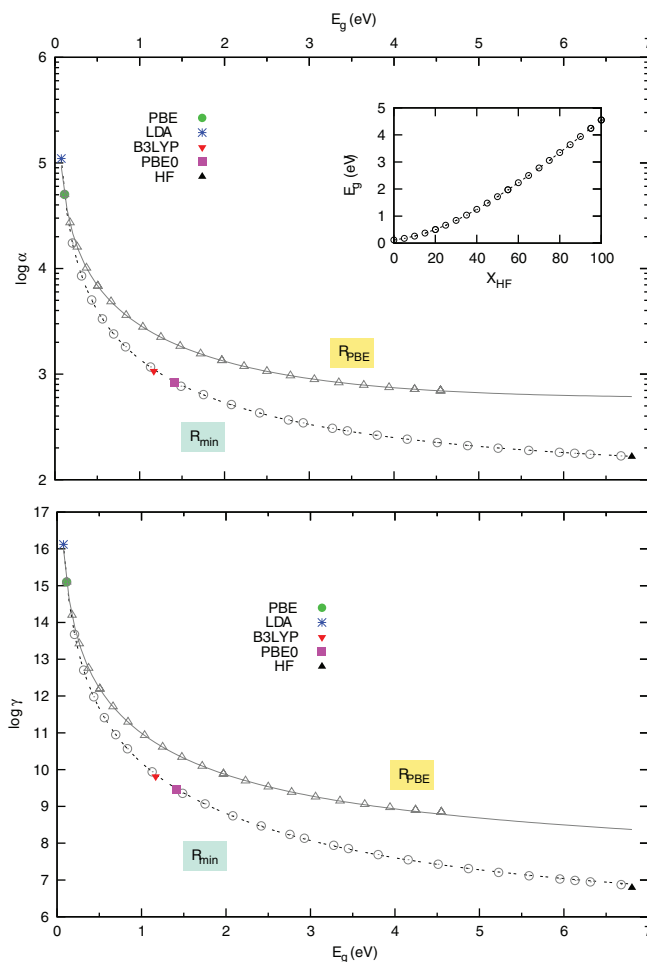

FIG. 5. Longitudinal polarizability α_{xx} (top) and second hyperpolarizability γ_{xxxx} (bottom) of PA (in a.u.) as functions of the energy gap E_g (eV) values obtained using different percentages of exact exchange X_{HF} within the PBE functional. Series R_{min} (circles) refers to CPKS calculations performed after geometry relaxation; series R_{PBE} (triangles) refers to CPKS calculations performed on the PBE relaxed geometry. LDA, B3LYP, and HF values of α_{xx} and γ_{xxxx} are indicated with colored points.

PBE0 calculation on structure R_{PBE}. The PBE BLA (0.009 Å) is much smaller than that associated with geometry relaxation (0.056 Å). Such a difference reverberates on a two times decrease of the band gap ($E_g(R_{PBE}) = 0.663$ eV vs $E_g(R_{min}) = 1.412$ eV), whereas $\alpha_{xx}(X_{HF} = 25\%; R_{PBE})$ increases by about two times and $\gamma_{xxxx}(X_{HF} = 25\%; R_{PBE})$ by almost 10 times. At $X_{HF} = 100\%$, the ratio over the HF values raises up to 4 for α_{xx} and about 40 for γ_{xxxx}.

C. Effect of the basis set

The effect of the basis set has been explored by progressively adding one, two, and three sets of polarization functions to the Pople's 6-31G basis used for all the calculations previously discussed. Both HF and DFT (PBE0) trends have been explored. Table X shows that only the first set of polarization functions (d on carbon atoms, p on hydrogen atoms) has an important effect on (hyper)polarizabilities, when added to the 6-31G set at the HF level - α_{xx} and γ_{xxxx} reduce by 8% and 32%, respectively - as a result of the increase of the band gap by about 5%. Adding a first set of polarization functions

TABLE IX. The effect of geometry on the calculation of the polarizability α_{xx} and the second hyperpolarizability γ_{xxxx} of PA. Values of the optical properties at different band gaps E_g (eV) have been obtained using i. the Hamiltonians indicated in parentheses (column E_g) at the relaxed geometry - column Calc(R_{min}); ii. the fitting functions $\alpha_{xx}(E_g)$ and $\gamma_{xxxx}(E_g)$ defined at the minimum PBE energy structures for variable exact exchange percentages $0 < X_{HF} < 100\%$ values - Fit(R_{min}); iii. and the fitting functions $\alpha_{xx}(E_g)$ and $\gamma_{xxxx}(E_g)$ defined for $X_{HF} = 0\%$ - Fit(R_{PBE}). Columns 10^x report the orders of magnitude relative to α_{xx} and γ_{xxxx}.

		α_{xx}				γ_{xxxx}			
	E_g	Calc(R_{min})	Fit(R_{min})	Fit(R_{PBE})	10^x	Calc(R_{min})	Fit(R_{min})	Fit(R_{PBE})	10^x
0.076	(LDA)	11.00	10.67	8.997	10^4	1.323	1.232	1.526	10^{16}
0.114	(PBE)	5.030	5.018	5.021	10^4	1.267	1.255	1.391	10^{15}
1.167	(B3LYP)	1.069	1.108	2.421	10^3	6.515	7.400	53.54	10^9
1.412	(PBE0)	8.343	8.063	18.54	10^2	2.866	2.573	22.38	10^9
6.805	(HF)	1.652	1.666	6.047	10^2	6.161	7.736	236.4	10^6

to basis set 6-31G (Table X, line 2) enlarges the PBE0 band gap by 2% and consequently reduces the polarizability by the same percentage amount and the second hyperpolarizability by about 13%. Again, further additions of polarization functions to the Pople's 6-31G basis set show a negligible effect.

Improving the valence part of Pople's 6-31G basis set by spreading its Gaussian functions or adding very diffuse *sp* shells would lead to numerical problems of *pseudo*-linear dependence in periodic calculations.[39] For this reason we have tested the performance of a multiple-zeta basis set series as well (Table X, bottom). Using much more diffuse *s* (for H) and *p* (for C) shells (than those of basis set 6-31G) within the valence description does not significantly alter the previous outline: overall, the variation along the rows, excluding the first entry, does not exceed 4(2)% for the HF (PBE0) polarizability and 9(5)% for the HF (PBE0) hyperpolarizability calculated along the chain axis. The most important changes occur when switching from the DZP basis set to the TZP basis set: α_{xx} and γ_{xxxx} decrease by 4% and 16% (HF) and 8% and 22% (PBE0), respectively.

However, comparing bases 6-31G(*d,p*) and TZP on a qualitative level, differences turn to be relatively small, apart from γ_{xxxx} PBE0 which decreases by about 16% using the TZP set. Moreover, whereas the ratio $\alpha_{PBE0}/\alpha_{HF}$ is about 5 for all the basis sets considered here, $\gamma_{PBE0}/\gamma_{HF}$ is more sensi-

tive to the basis set used. Nevertheless, choice of the 6-31G basis set for most of the present calculations was important to allow comparison with data reported in the literature. It is also worth noting that the DFT overestimation of the second hyperpolarizability is further amplified by addition of polarization functions to the 6-31G basis set (from 25% to 30%) or using more extended multiple-zeta basis sets (from 10% to 15%).

V. CONCLUSIONS

The longitudinal polarizability α_{xx} and second hyperpolarizability γ_{xxxx} of polyacetylene have been evaluated with five different Hamiltonians. The numerical system developed in this work depends upon the choice of computational parameters that are more stringent the smaller the energy gap. Convergence with respect to the number of $\vec{k}$ points used in the various steps of the calculation (SCF, CP-SC1, and CP-SC2) is not readily reached: up to 1200 $\vec{k}$ points are required in the worst case, namely, γ_{xxxx} evaluated within the local density approximation, providing a band gap as small as 3 millihartree.

Also the range of the exact exchange term (used in B3LYP, PBE0, and HF) strongly depends on the band gap, which is relatively small for the two hybrid functionals (1.1-

TABLE X. Effect of the basis set on the calculation of the polarizability α_{xx} and the second hyperpolarizability γ_{xxxx} of PA. Columns 2–7 provide the exponents (bohr^{-2}) of the polarization functions added to the 6-31G and DZP sets (see Refs. 54 and 55 for a complete definition). The exponents of the most diffuse functions are $s_H = 0.16$ and $sp_C = 0.17$ for the 6-31G set and $s_H = 0.12$, $s_C = 0.16$ and $p_C = 0.12$ for the DZP set. γ_{xxxx} in 10^9 (PBE0) and 10^6 (HF) a.u. Energy gaps E_g in eV. Calculations have been performed at the optimized geometries. Other computational parameters as in previous tables.

	H			C			PBE0			HF		
BS	p_1	p_2	d	d_1	d_2	f	E_g	α_{xx}	γ_{xxxx}	E_g	α_{xx}	γ_{xxxx}
6-31G	...	...	...	...	...	...	1.434	834.3	2.8658	6.827	165.2	6.161
6-31G(*p,d*)	1.10	...	...	0.80	...	...	1.461	818.2	2.5005	7.186	151.2	4.220
6-31G(2*d*,2*p*)	2.10	0.75	...	2.50	0.63	...	1.464	818.7	2.4694	7.235	151.2	4.092
6-31G(2*df*,2*pd*)	2.10	0.75	1.00	2.50	0.63	0.80	1.478	806.2	2.3454	7.252	151.0	4.030
DZP	1.00	...	...	0.75	...	...	1.448	840.6	2.6834	7.067	156.3	4.687
TZP	1.00	...	...	0.75	...	...	1.502	774.5	2.0947	7.140	149.3	3.916
TZPP	1.41	0.59	1.06	1.10	0.52	0.76	1.494	792.5	2.1861	7.165	154.9	4.275
QZVP	1.00	...	...	0.75	...	...	1.502	774.6	2.0847	7.156	151.2	4.130
QZVPP	1.41	0.59	1.06	1.10	0.52	0.76	1.497	790.5	2.1598	7.167	154.6	4.235

1.4 eV vs 6.8 eV for HF). As a matter of fact, exchange interactions within a radius of about 130 Å must be considered in the first case, whereas only 40 Å are required for HF.

It has been shown that the use of oligomers as a model for polymers can be very misleading, as the convergence with m - the number of monomers in the chain - can be quite slow when the gap is small, as for LDA, PBE, PBE0, and B3LYP. In these cases the results at $m = 50$ still differ from the polymer limit by 1% (α) or 17% (γ) (PBE0 or B3LYP), or by several orders of magnitude (LDA or PBE). Results have been shown to strongly depend on the adopted Hamiltonian (for γ the difference can be as large as 10 orders of magnitude), and on the resulting band gap.

Literature data concerning short oligomer chains indicate that Hartree-Fock (hyper)polarizabilities are close to the ones obtained with correlated wave functions. On this basis our LDA and GGA data give catastrophically exaggerated values (DFT *catastrophe*), whereas hybrid data are more reasonable but still far apart by orders of magnitude when γ_{xxxx} is considered. LR corrections[52,53] have been claimed, in the case of finite oligomer chains, to limit catastrophic divergence on (hyper)polarizabilities, but still performance depends parametrically on the system[52] and no clear improvements of LR corrected functionals over HF have been shown.[52,53]

Besides the wide family of small-gap organic polymers, there is a connection with the optical properties of more complex systems such as carbon nanotubes (CNT) (1D systems characterized by a small band gap). Thus, the present work is preliminary to a systematic study of the (hyper)polarizabilities of CNT.

ACKNOWLEDGMENTS

[1] B. Champagne, E. A. Perpéte, S. J. A. van Gisbergen, E. J. Baerends, J. Snijders, C. Soubra Ghaoui, K. A. Robins, and B. Kirtman, J. Chem. Phys. **109**, 10489 (1998).

[2] B. Champagne, E. A. Perpéte, S. J. A. van Gisbergen, E. J. Baerends, J. Snijders, C. Soubra Ghaoui, K. A. Robins, and B. Kirtman, J. Chem. Phys. **110**, 11664 (1999).

[3] S. J. A. van Gisbergen, P. R. T. Schipper, O. V. Gritsenko, E. J. Baerends, J. G. Snijders, B. Champagne, and B. Kirtman, Phys. Rev. Lett. **83**, 694 (1999).

[4] B. Champagne, E. Perpéte, D. Jacquemin, S. van Gisbergen, E. Baerends, C. Soubra Ghaoui, K. Robins, and B. Kirtman, J. Phys. Chem. A **104**, 4755 (2000).

[5] S. Kümmel, L. Kronik, and J. P. Perdew, Phys. Rev. Lett. **93**, 213002 (2004).

[6] M. van Faassen, P. de Boeij, R. van Leeuwen, J. Berger, and J. Snijders, Phys. Rev. Lett. **88**, 186401 (2002).

[7] M. van Faassen, P. de Boeij, R. van Leeuwen, J. Berger, and J. Snijders, J. Chem. Phys. **118**, 1044 (2003).

[8] R. Dovesi, V. R. Saunders, C. Roetti, R. Orlando, C. M. Zicovich Wilson, F. Pascale, K. Doll, N. M. Harrison, B. Civalleri, I. J. Bush, Ph. D'Arco, and M. Llunell, CRYSTAL09 *User's Manual*, Università di Torino, Torino (2009).

[9] M. Ferrero, M. Rérat, R. Orlando, and R. Dovesi, J. Chem. Phys. **128**, 014110 (2008).

[10] M. Springborg, V. Tevekeliyska, and B. Kirtman, Phys. Rev. B **82**, 165442 (2010).

[11] M. Springborg and B. Kirtman, Theor. Chem. Acc. **130**, 687 (2011).

[12] G. J. B. Hurst, M. Dupuis, and E. Clementi, J. Chem. Phys. **89**, 385 (1988).

[13] B. Kirtman, F. L. Gu, and D. M. Bishop, J. Chem. Phys. **113**, 1294 (2000).

[14] M. Ferrero, M. Rérat, R. Orlando, and R. Dovesi, J. Comput. Chem. **29**, 1450 (2008).

[15] M. Ferrero, M. Rérat, B. Kirtman, and R. Dovesi, J. Chem. Phys. **129**, 244110 (2008).

[16] M. Ferrero, M. Rérat, R. Orlando, R. Dovesi, and I. Bush, J. Phys. Conf.: Ser. **117**, 12016 (2008).

[17] P. Otto, Phys. Rev. B **45**, 10876 (1992).

[18] P. Otto, F. L. Gu, and J. Ladik, J. Chem. Phys. **110**, 2717 (1999).

[19] K. N. Kudin and G. Scuseria, J. Chem. Phys. **113**, 7779 (2000).

[20] A. F. Izmaylov, E. N. Brothers, and G. Scuseria, J. Chem. Phys. **125**, 224105 (2006).

[21] M. Springborg and B. Kirtman, J. Chem. Phys. **126**, 104107 (2007).

[22] R. Orlando, V. Lacivita, R. Bast, and K. Ruud, J. Chem. Phys. **132**, 244106 (2010).

[23] B. Kirtman, J. L. Toto, K. A. Robins, and M. Hasan, J. Chem. Phys. **102**, 5350 (1995).

[24] P. A.M. Dirac, Math. Proc. Cambridge Philos. Soc. **26**, 376 (1930).

[25] W. Kohn and L. J. Sham, Phys. Rev. **140**, A1133 (1965).

[26] S. H. Vosko, L. Wilk, and M. Nusair, Can. J. Phys. **58**, 1200 (1980).

[27] J. P. Perdew, K. Burke, and M. Ernzerhof, Phys. Rev. Lett. **77**, 3865 (1996).

[28] B. Hammer, L. B. Hansena, and J. K. Nrskov, Phys. Rev. B **59**, 7413 (1999).

[29] C. Adamo and V. Barone, J. Chem. Phys. **116**, 5933 (2002).

[30] Y. Zhang and W. Yang, Phys. Rev. Lett. **80**, 890 (1998).

[31] C. Adamo and V. Barone, J. Chem. Phys. **110**, 6158 (1999).

[32] A. D. Becke, J. Chem. Phys. **98**, 5648 (1993).

[33] C. Lee, W. Yang, and R. G. Parr, Phys. Rev. B **37**, 785 (1988).

[34] P. J. Stephens, F. J. Devlin, C. F. Chabalowski, and M. J. Frisch, J. Phys. Chem. **98**, 11623 (1994).

[35] C. Fincher, C. Chen, A. Heeger, A. MacDiarmid, and J. Hastings, Phys. Rev. Lett. **48**, 100 (1982).

[36] R. Dovesi, C. Pisani, C. Roetti, and V. Saunders, Phys. Rev. B **28**, 5781 (1983).

[37] V. R. Saunders, C. Freyria Fava, R. Dovesi, L. Salasco, and C. Roetti, Mol. Phys. **77**, 629 (1992).

[38] V. R. Saunders, C. Freyria Fava, R. Dovesi, and C. Roetti, Comput. Phys. Commun. **84**, 156 (1994).

[39] B. Champagne, D. Jacquemin, F. Gu, Y. Aoki, B. Kirtman, and D. Bishop, Chem. Phys. Lett. **373**, 539 (2003).

[40] M. Causá, R. Dovesi, R. Orlando, C. Pisani, and V. R. Saunders, J. Phys. Chem. **92**, 909 (1988).

[41] A. D. Becke, J. Chem. Phys. **88**, 2547 (1988).

[42] M. D. Towler, A. Zupan, and M. Causá, Comput. Phys. Commun. **98**, 181 (1996).

[43] T. T. Toto, J. L. Toto, C. P. de Melo, M. Hasan, and B. Kirtman, Chem. Phys. Lett. **244**, 59 (1995).

[44] D. Lu, B. Marten, M. Ringnalda, R. A. Friesner, and W. A. Goddard III, Chem. Phys. Lett. **257**, 224 (1996).

[45] B. Kirtman, B. Champagne, F. Gu, and D. Bishop, Int. J. Quantum Chem. **90**, 709 (2002).

[46] P. Limacher, K. Mikkelsen, and H. Luthi, J. Chem. Phys. **130**, 194114 (2009).

[47] C. Yannoni and T. Clarke, Phys. Rev. Lett. **51**, 1191 (1983).

[48] H. Kahlert, O. Leitner, and G. Leising, Synth. Met. **17**, 467 (1987).

[49] H. Guo and J. Paldus, Int. J. Quantum Chem. **63**, 345 (1997).

[50] E. Perpète and B. Champagne, J. Mole. Struct.: THEOCHEM **487**, 39 (1999).

[51] A. Karolewski, R. Armiento, and S. Kümmel, J. Chem. Theory Comput. **5**, 712 (2009).

[52] H. Sekino, Y. Maeda, M. Kamiya, and K. Hirao, J. Chem. Phys. **126**, 014107 (2007).

[53] B. Kirtman, S. Bonness, A. Ramirez Solis, B. Champagne, H. Matsumoto, and H. Sekino, J. Chem. Phys. **128**, 114108 (2008).

[54] A. J. Thakkar, T. Koga, M. Saito, and R. E. Hoffmeyer, Int. J. Quantum Chem., Symp. **48**, 343 (1993).

[55] A. Schafer, H. Horn, and R. M. Alrichs, J. Chem. Phys. **97**, 2571 (1992).